Macromolecular Research, Vol. 19, No. 4, pp 370-378 (2011)
DOI 10.1007/s13233-011-0409-8
www.springer.com/13233

Fabrication and Characterization of Coaxial Electrospun Polyethylene Glycol/ Polyvinylidene Fluoride (Core/Sheath) Composite Non-Woven Mats

Thuy Thi Thu Nguyen[1], Jae Goo Lee[2], and Jun Seo Park*[,1]

[1]*Graduate School and Division of Chemical Engineering, Hankyong National University, Gyeonggi-do 456-749, Korea*
[2]*Clean Fossil Fuel Research Center, Korea Institute of Energy Research, Daejeon 305-343, Korea*

Received August 19, 2010; Revised November 8, 2010; Accepted November 19, 2010

Abstract: Polyethylene glycol (PEG) is a phase change material (PCM) with a high heat of fusion and is capable of storing and releasing large amounts of energy at its melting and crystallization point as the surrounding temperature changes. This study deals with the fabrication of polyethylene glycol/polyvinylidene fluoride (PVDF) core/sheath non-woven mats by coaxial electrospinning and characterization of the obtained mats. The non-woven mats comprised of nanofibers (average diameter: ~700 nm) in which PEG (PCM) was encapsulated with a PVDF sheath. The PVDF sheath helped prevent PEG leakage from the fibers during a phase change and protected the core from an external environment. Water contact angle (WCA) measurements, attenuated total reflectance-Fourier transform infrared (ATR-FTIR) spectroscopy measurements, X-ray photoelectron spectroscopy (XPS) analysis and transmission electron microscopy (TEM) studies confirmed that the fabricated mats comprised a PEG layer covered with a PVDF layer. The thermal properties of the mats were analyzed by differential scanning calorimetry (DSC) and thermogravimetric analysis (TGA). These results suggest that the PEG/PVDF core/sheath non-woven mats have good thermal reliability and sufficiently high tensile strength with potential applications in the manufacture of thermo-regulated textiles.

Keywords: coaxial electrospinning, phase change material, polyethylene glycol, thermal properties, energy storage.

Introduction

The need for developing renewable and clean energy sources has resulted in increased focus on phase change materials (PCMs). PCMs undergo a reversible phase change; hence, they absorb energy upon heating and release the absorbed energy to the environment during cooling.[1-4] However, PCMs have certain inherent disadvantages such as density change, phase segregation, low thermal conductivity, and leaking during phase change. Because of these properties, it is very difficult to use them directly as heat storage materials.[5] Intensive studies have been carried out to develop new methods for producing PCMs that do not have the abovementioned disadvantages. Such PCMs can be used in various new applications such as manufacture of smart textiles and thermo-regulated fibers.[6-8] Some of the convenient methods for incorporating PCMs into fabrics are coating, lamination, melt spinning, and bi-component synthetic fiber extrusion. Recently, there has been increased attention to the production of PCM microcapsules, which are used in the pre-processing stage in the afore-mentioned method for the fabrication of thermo-regulated fibers, fabrics etc. Microencapsulated PCMs comprise submicron- to several micron-sized particles. The PCM acts the core material, and it is enwrapped by a coating layer or a polymer membrane.[9-12] Because of the small diameter of the constituent particles, the surface-area-to-volume ratio of microencapsulated PCMs is high, and their thermal conductivity is well enhanced.[13] Alkan *et al.*[14] prepared microcapsules comprising poly (methyl methacrylate) (PMMA) as the shell material and docosane as the core by emulsion polymerization. The prepared microcapsules had a smooth and compact surface and an average diameter of 0.16 μm; further, the enthalpy of microcapsules containing 28 wt% docosane was 54.6 J/g. Sarl *et al*.[5] used the same method to prepare PMMA microcapsules with an average n-octacosane composition of 43 wt%.

Recently, many attempts have been made to prepare thermo-regulated composite fibers or fabrics by electrospinning.[8,15,16] Electrospinning involves the use of electrostatic force to draw a polymer solution into fibers whose diameters vary from a few nanometers to several micrometers.[17-20] Thermo-regulated composite fibers are fabricated by direct electrospinning of a PCM/polymer blend solution. Non-woven mats comprising a PCM and supporting materials (polymers) have attractive advantages such as desirable dimensions, high latent heat, mechanical strength and spe-

*Corresponding Author. E-mail: jspark@hknu.ac.kr

cific surface area. Further, these non-woven mats can be directly used in various applications without the need for additional encapsulation. Chen *et al*.[16] used electrospinning to fabricate novel polymer-based shape-stabilized ultrafine PCM fibers from a lauric acid/polyethylene terephthalate (PET) composite. In these fibers, lauric acid and PET acted as the PCM and the polymer matrix, respectively. These composite fibers had high latent heats of melting and crystallization (70.76 and 62.14 J/g, respectively) and showed excellent mechanical performance. Chen *et al*.[8] also reported the fabrication of ultrafine fibers of a polyethylene glycol (PEG)/cellulose acetate (CA) composite. For further improvement of the thermal stability and water resistance of the electrospun PEG/CA composite fibers, surface cross-linking of the fibers was carried out using toluene-2,4-diisocyanate (TDI) as the cross-linking agent.[15] While this cross-linking led to an improvement of the thermal stability of the fibers, it caused the enthalpy of the cross-linked fibers to become lesser than that of the original electrospun fibers. In general, composite spinning (spinning of a polymer/PCM solution) is a simple method for fabricating thermo-regulated fibers that have high latent heat. Nevertheless, a shortcoming of the fibers fabricated by this method is the loss of the constituent PCMs after repeated use. McCane *et al*.[21] developed a method based on melt coaxial electrospinning for fabricating non-woven mats containing PCMs. This method allows a non-polar solid PCM such as paraffin to be electrospun and encapsulated in one step. In the above-mentioned type of non-woven mats, octadecan (45 wt%) formed the core, which was protected by a polymer sheath.

A large number of organic, inorganic, and eutectic materials have been identified as PCMs on the basis of their melting temperatures and latent heats.[22-24] The organic PCM group, which includes parafins, fatty acids, and PEGs, has certain advantageous properties such as high heat of fusion, good chemical stability, availability over in wide temperature range, and ability to be frozen without super cooling. PEG is a polyether compound that is widely utilized as a PCM, especially in textile applications. The thermal storage capacity and melting point of PEG vary depending on its molecular weight.[25,26] Polyvinylidene fluoride (PVDF) is a semi-crystalline polymer with high mechanical strength and good thermal properties. Therefore, PVDF is a promising material for a supporting polymer that can help maintain the shape of the fibers and prevent PEG leakage from the fibers during the phase change process.

Coaxial electrospinning is based on the electrospinning principle, and it involves the use of a spinneret composed of two coaxial capillaries for the fabrication of a continuous double layer of nanofibers.[27-29] Till date, there has been no report on the preparation of PCM/polymer nonwoven mats by coaxial electrospinning. In this study, PEG/PVDF core/sheath nonwoven mats were prepared by coaxial electrospinning; in these mats, PEG formed the core and PVDF acted as the sheath. This core/sheath nonwoven mat has the following advantages: (1) the PCM (PEG) can be locked within the fibers without any need for subsequent fiber processing; (2) the PVDF sheath helps prevent PEG leakage during phase change and protects the core from external environment; and (3) the mat has a large heat-transfer area, and its volume remain constant during phase change. The structure of the core/sheath nanofibers was confirmed by water contact angle (WCA) measurements, attenuated total reflectance-Fourier transform infrared (ATR-FTIR) spectroscopy studies and transmission electron microscopy (TEM) observations. The morphology of the electrospun PEG/PVDF core/sheath nanofibers was determined from field-emission scanning electron microscopy (FE-SEM) images. Differential scanning calorimetry (DSC) and thermogravimetric analysis (TGA) were employed to investigate the thermal properties of the prepared PEG/PVDF core/sheath nanofibers. A DSC thermal cycling test was conducted to determine the thermal reliability of the prepared nanofibers. In addition, the tensile properties of the PEG/PVDF core/sheath non-woven mats were evaluated.

Experimental

Materials. PEGs with average molecular weights of 600 and 1,000 Da were purchased from Samchun Co. (Korea), while PEG with an average molecular weight of 8,000 Da was supplied by Alfa Aesav (a Johnson Matthey Co.). Kynar @761 PVDF was used. *N*,*N*-dimethyl acetamide (DMAc) and acetone (solvents) were purchased from Samchun Co. (Korea). All of the chemicals were used as such without further purification.

Coaxial Electrospinning. PVDF (15 wt%) was dissolved in a mixture of DMAc and acetone (60:40, w/w). The same DMAc/acetone mixture was used for dissolving the above-mentioned three types of PEGs. The concentration of the PEG in the solutions ranged from 30 to 50 wt%.

In this study, the coaxial spinneret used consisted of two concentrically arranged capillaries. The inner capillary had an inner diameter (ID) of 0.35 mm and an outer diameter (OD) of 0.65 mm, while the outer capillary had an ID of 1.05 mm and an OD of 1.20 mm. A certain amounts of the PEG and PVDF solutions were contained in two individual syringes connected to the coaxial spinneret. The flow rates in the capillaries were controlled by two separate pumps. Both capillaries were connected to the same high voltage power supply. The fibers were collected on an aluminum foil placed above the flat grounded metal plate. The applied voltage and the distance between the tip of the spinneret and the collector were maintained at 12 kV and 13 cm, respectively. The sheath flow rate was set at 1.0 mL/h, while the core flow rate was varied from 0.09 to 0.12 mL/h. All the electrospinning processes were carried out at around 25 ºC.

Characterization. WCA measurements were carried out for pure PVDF non-woven mats and PEG/PVDF core/sheath non-woven mats prepared at different core feed rates, in order to identify possible differences between the wetting abilities of these mats. The WCAs of the non-woven mats were measured using a video contact angle instrument (Samsung FA-CED camera, Korea). The contact angles were measured immediately after deionized water was allowed to fall freely onto the surfaces of the flat non-woven mats. The obtained contact angle in each case was the average of the values recorded in five measurements carried out at different locations of the non-woven mat surface. The configuration of the core/sheath structure in the coaxially electrospun nanofibers was determined by a FTIR analysis (JASCO, ATR FTIR 6100, Japan) and X-ray photoelectron spectroscopy (XPS, Thermo, MultiLab 2000).

The morphology of the non-woven mats was determined by field emission scanning electron microscopy (FE-SEM, HITACHI S-4700, Japan) observation carried out using a coating system (BAL-TEC MED020). The fiber diameter ranges and average fiber diameters of the non-woven mats were measured from the FE-SEM photographs using the visualization software (TOMORO ScopeEye 3.6).

TEM observations (TecnaiG^2, USA) were carried out using carbon-coated copper grids to determine the core/sheath structure of the coaxially electrospun fibers.

The thermal properties of the PEG-PVDF core-sheath non-woven mats, such as melting and crystallization points and latent heats, were measured by DSC (SH IN2920, TA instruments, USA). The analyses were carried out at a heating rate of 10 °C/min under a constant stream of nitrogen (flow rate: 70 mL/min). In order to determine the thermal reliability of the PEG-PVDF core-sheath non-woven mats, a thermal cycling test involving 100 consecutive melting and freezing cycles was conducted.

A TGA experiment was carried out using a thermal analyzer (EXSTAR 6000, Seiko instruments Inc, USA), which was calibrated from 30 to 650 °C at a heating rate of 20 °C/min.

The mechanical performance of the nanofiber membranes was characterized by tensile testing in a tensile tester (LR 5K, LLOYD instrument) with a load cell of 10 N.

Results and Discussion

Selection of PEGs for the Coaxial Electrospinning. PEG, a typical solid-liquid phase change material, is a linear polymer containing $(CH_2\text{-}O\text{-}CH_2)_n$ units on the chain and hydroxyl groups on two ends. It can be easily crystallized and has a large latent heat. PEG with different molecular weights of have different physical properties such as viscosity, melting and crystallization points, and latent heat. In this study, we compared the physical properties and coaxial electrospinning abilities of three types of PEGs: PEG 600, PEG 1000, and PEG 8000. The numbers that are included in the names indicate the average molecular weights, for example, PEG with an average molecular weight of approximately 600 Da is labeled PEG 600. The thermal properties of these PEGs are summarized in Table I. The relation between the viscosities and concentrations of the three PEG solutions is presented in Figure 1. The maximum amounts of PEG 600, PEG 1000, and PEG 8000 that could be dissolved completely in the DMAc/acetone (60:40, w/w) mixture at 25 °C were 90, 60, and 30 wt%, respectively.

From Table I, it is apparent that the melting and crystallization points of the PEGs increased significantly with the average molecular weight. Further the latent heat of PEG 1000 was much higher than that of PEG 600. However, there was negligible difference between the latent heats of PEG 1000 and PEG 8000. Since the aim of this study is to fabricate PEG/PVDF core/sheath nanofibers with high energy storage capacity, we consider PEG 1000 and PEG 8000 to

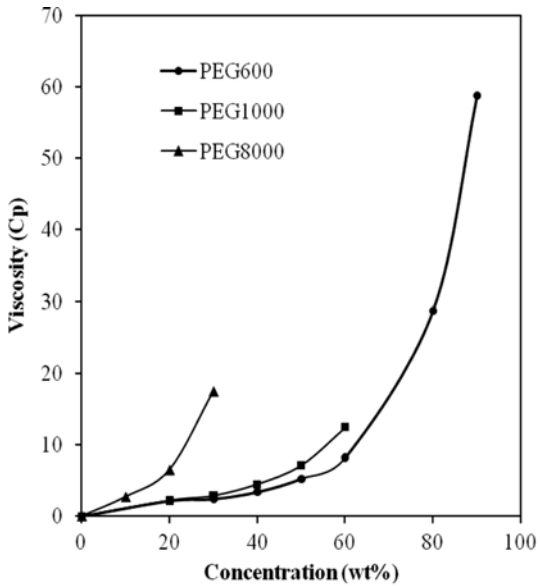

Figure 1. Relation between the viscosities and concentrations of PEG 600, PEG 1000, and PEG 8000 solutions.

Table I. Thermal Properties of PEG 600, PEG 1000, and PEG 8000

PEG	Melting Point (°C) (Onset Temperature)	Latent Heat of Melting (J/g)	Crystallization Point (°C) (Onset Temperature)	Latent Heat of Crystallization (J/g)
PEG 600	16.5	112.8	14.1	108.8
PEG 1000	34.9	171.9	27.6	168.0
PEG 8000	61.6	173.6	45.4	165.7

be suitable for use as PCMs.

Figure 1 shows the dependence of the viscosity of the PEG solution on the PEG molecular weight. The viscosity of the solution containing 30 wt% PEG 8000 was higher than that of solution containing 60 wt% PEG 1000. This is one of the reasons for the fabrication of PEG/PVDF core/sheath nanofibers using PEG 8000 as the core material being unsuccessful. The high viscosity of the charged polymer jets may increase the degree of bending instability in electrospinning process.[30] For the fabrication of PEG/PVDF core/sheath nanofibers, a 50 wt% solution of PEG 1000 was employed as a core solution.

Effect of Core Feed Rate on the Fabrication of PEG/PVDF Core/Sheath Nanofibers. The flow rate of the electrospinning solution is an important controlled variable parameter, especially in coaxial electrospinning. To maintain a continuous core/sheath structure, the core and sheath solutions should be pumped at appropriate flow rates. If the feed rate of the core solution is too high, the core fluid jet would break into droplets. Some researchers have highlighted that the sheath fluid encapsulated and stretched the core fluid into fine fibers.[31-33] Hence, it may thus be essential to maintain the sheath fluid at a sufficiently rate. In this experiment, coaxial electrospinning was carried out at a constant sheath feed rate of 1 mL/h, whereas the core feed rate was varied from 0.09 to 0.12 mL/h. The configuration of the double layer for the core/sheath fibers was identified by WCA measurement. Since PEG is highly hydrophilic, its presence in the sheath layer of the PEG/PVDF fibers fabricated by coaxial electrospinning brings about a decrease in the hydrophobicity of the fibers. Figure 2 shows the WCAs of the pure PVDF and PEG/PVDF non-woven mats fabricated by coaxial electrospinning at different core feed rates.

The WCA measurement data in Figure 2 indicates that the pure PVDF non-woven mat had a hydrophobic surface. The average contact angle made by the water droplets on the surface of the pure PVDF non-woven mat was 107.6°. The WCAs obtained for the PEG/PVDF non-woven mats fabricated by coaxial electrospinning at core feed rates of 0.09 and 0.108 mL/h (107.4° and 104.9°, respectively) were similar to the WCA obtained for the pure PVDF mat. When the core feed rate was 0.12 mL/h, the WCA of the PEG/PVDF non-woven mat decreased significantly, indicating the presence of PEG on the surface of the nanofibers. This was because of the following reason: the amount of sheath solution was not sufficient for encapsulating the core solution, and hence, the core and sheath solutions diffused into each other at the spinneret tip. On the basis of the experiment results, we concluded that the optimal core feed rate for the fabrication of PEG/PVDF core/sheath nanofibers at the sheath feed rate of 1 mL/h was 0.108 mL/h.

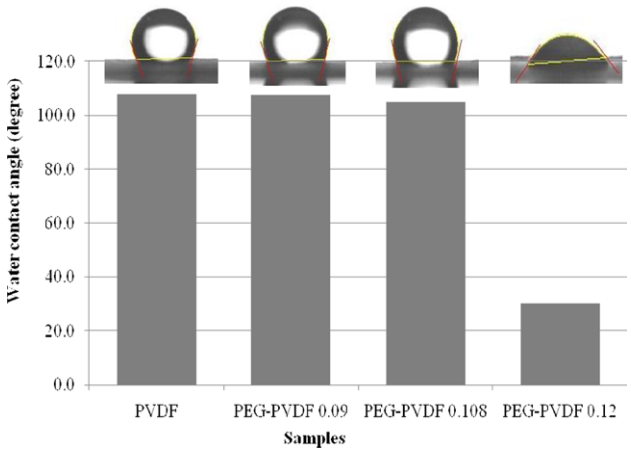

Figure 2. WCAs of pure PVDF and PEG/PVDF non-woven mats fabricated by coaxial electrospinning at different core feed rates (the inserted pictures show the shapes of the water droplets on the surface of the non-woven mats).

ATR-FTIR and XPS have been widely used to study surface composition. Therefore, they were effective methods to confirm the formation of the double layer of PEG/PVDF core/sheath nanofibers. Figure 3 shows the ATR-FTIR spectra of the pure PVDF non-woven mat and the PEG/PVDF non-woven mats fabricated by coaxial electrospinning at different core feed rates. The ATR-FTIR spectra of the PEG/PVDF non-woven mats prepared by coaxial electrospinning at core feed rates of 0.09 and 0.108 mL/h were very similar to that of the pure PVDF mat, indicating that the outer layer of the core/sheath fibers was pure PVDF. When the core feed rate was 0.12 mL/h, a new peak corresponding to C-O stretching vibration was observed at 1113 cm^{-1} in the FTIR spectrum of the PEG/PVDF non-woven mat. PEG has C-O bonds, while PVDF does not. Therefore, the appearance of the aforesaid peak confirmed that the surface of the nanofibers contained not only PVDF but also PEG. This indicates that the core/sheath structure of the PEG/PVDF nanofibers disintegrated when the core feed rate was 0.12 mL/h. This result was consistent with the results of WCA measurements.

Figure 4 shows the XPS survey spectra of the pure PVDF non-woven mat and coaxial electrospun PEG/PVDF non-

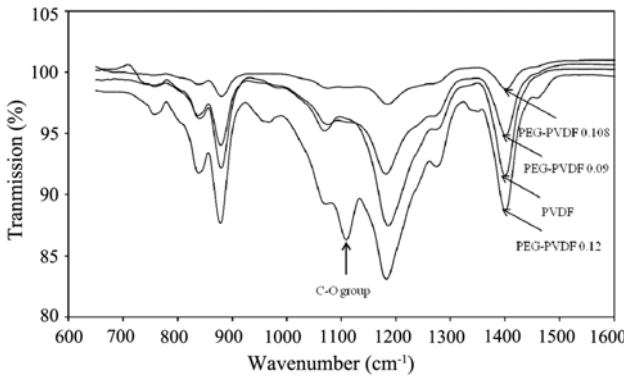

Figure 3. ATR-FTIR spectra of pure PVDF non-woven mat and PEG/PVDF non-woven mats fabricated by coaxial electrospinning at different core feed rates.

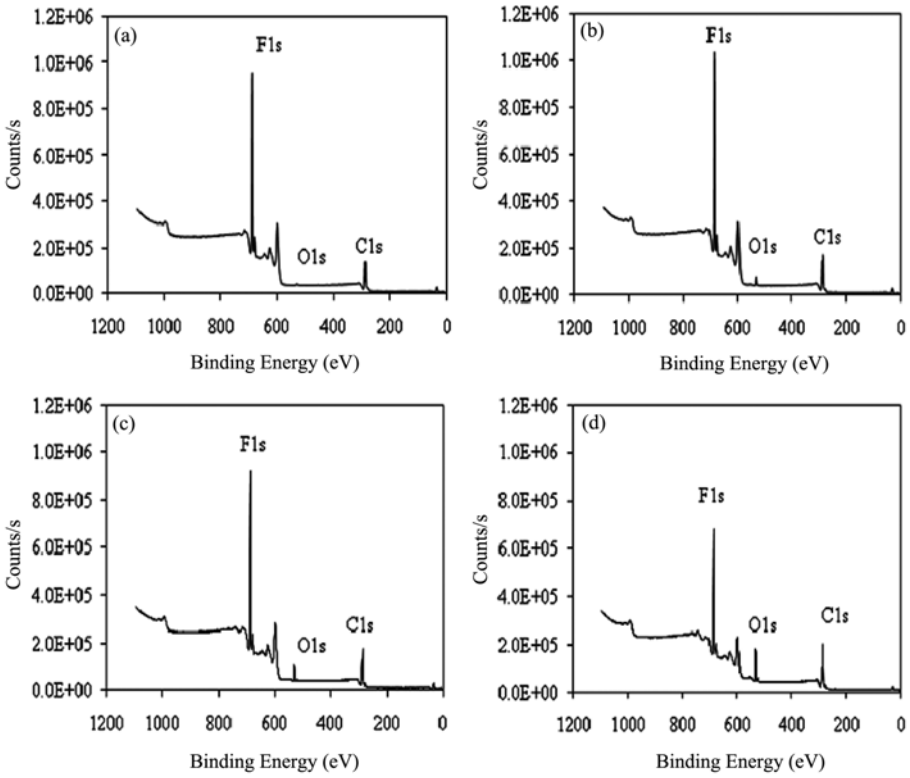

Figure 4. XPS results obtained for (a) PVDF and PEG/PVDF coaxial electrospun fibers fabricated at core feed rates of (b) 0.09 mL/h, (c) 0.108 mL/h, and (d) 0.12 mL/h.

woven mats. PVDF does not contain oxygen atom but PEG does. Hence, the absence of the O1s peak in the XPS survey spectrum would indicate the formation of PEG/PVDF fibers with a core/sheath structure. It could be seen that F1s and C1s peaks appeared in the spectrum of the electrospun PVDF and PEG/PVDF non-woven mats. In the case of electrospun nanofibers fabricated at core feed rate of 0.09 and 0.108 mL/h, the intensity of the O1s peaks in the XPS spectrum increased slightly. This increase in the intensity was attributed to the presence of several blended PEG/PVDF nanofibers that could not be identified by WCA measurement and FTIR analysis. When the core feed rate was increased to 0.12 mL/h, there was a significant increase in the O1s peak intensity, which suggested that PEG was mostly on the shell of nanofibers, rather than forming their core. Similar phenomena of XPS analysis were reported by Sun *et al*.[32] and Zhao *et al*.[34]

FE-SEM images demonstrating the effect of core feed rate on the morphology of the electrospun fibers are shown in Figure 5. The average diameters of the PVDF fibers and coaxially electrospun PEG/PVDF fibers are listed in Table II. It was found that the electrospun PVDF fibers had the smallest average diameter among all the coaxial electrospun fibers. When the feed rate of PEG solution was increased, the average diameter of the coaxial electrospun nanofibers increased. This phenomenon could be explained that an increase in the feed rate of the core fluid would result in an increase in the total amount of fluid jetting out of the coaxial spinneret. This in turn would cause an increase in the average diameter of the coaxial electrospun fibers. The diameter distribution of the coaxial electrospun fibers also became broader with

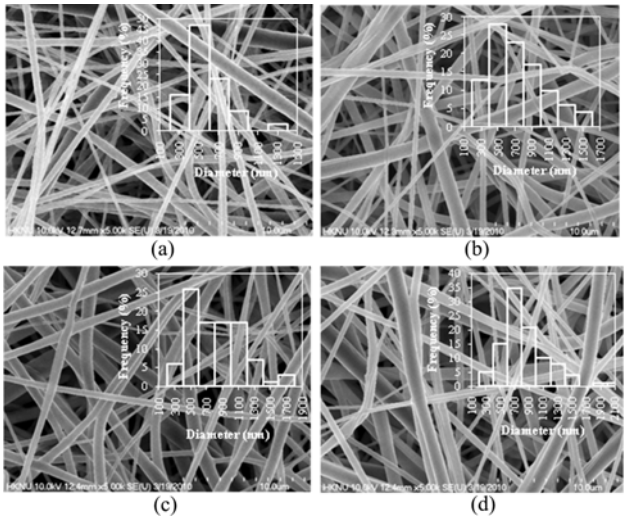

Figure 5. FE-SEM images of electrospun fibers and diameter distributions of (a) PVDF and PEG/PVDF coaxial electrospun fibers fabricated at core feed rates of (b) 0.09 mL/h, (c) 0.108 mL/h, and (d) 0.12 mL/h.

Table II. Average Diameters of PVDF Electrospun Fibers and PEG/PVDF Coaxial Electrospun Fibers Fabricated at Different Core Feed Rates

Type of Sample	Core Feed Rate (mL/h)	Average Diameter (nm)
PVDF	0	480
PEG/PVDF	0.09	644
PEG/PVDF	0.108	721
PEG/PVDF	0.12	737

an increase in the core feed rate. The diameters of the coaxial fibers were in the range 200 to 1,600 nm when the feed rate of the core fluid was 0.09 mL/h and in the range 200 to 2,100 nm when the feed rate was 0.12 mL/h. A similar phenomenon was reported by other researches who studied different core/sheath systems.[35,36] The aforementioned result could be attributed to the temporal instability of the core solution caused by an increase in the core feed rate under a high applied voltage. The smaller nanofibers in the non-woven mats were probably formed from the sub-jets that separated out from the main jet during the electrospinning process.

Core/Sheath Structure of Coaxially Electrospun PEG/PVDF Nanofibers. The structures of the PEG/PVDF nanofibers fabricated by coaxial electrospinning at different core feed rates were observed by TEM images (Figure 6). It could be seen in Figure 6(a) that when the core feed rate was 0.108 mL/h, the coaxial nanofibers had a relatively uniform core/sheath structure in which PEG was encapsulated by the PVDF layer. The interface between the core fibers and the sheath fibers was smooth, and a relatively thin sheath layer was observed. When the core feed rate was increased to 0.12 mL/h, the core/sheath structure was not detected (Figure 6(b)). This result demonstrated that the coaxial structure of the PEG/PVDF nanofibers degraded when the core feed rate was 0.12 mL/h.

Thermal Properties and Thermal Stability of PEG/PVDF Core/Sheath Non-Woven Mat. According to the WCA measurements results and ATR-FTIR spectra, a PEG/PVDF core/sheath non-woven mat with the maximum possible amount of PEG in the core was formed when the feed rates

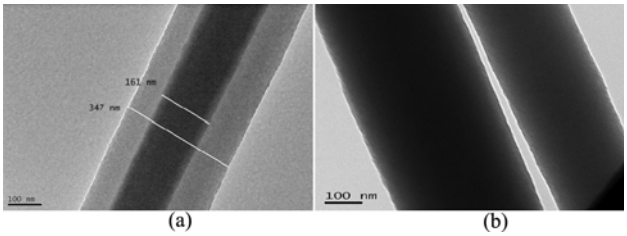

Figure 6. TEM images of coaxially electrospun PEG/PVDF nanofibers fabricated at core feed rates of (a) 0.108 and (b) 0.12 mL/h.

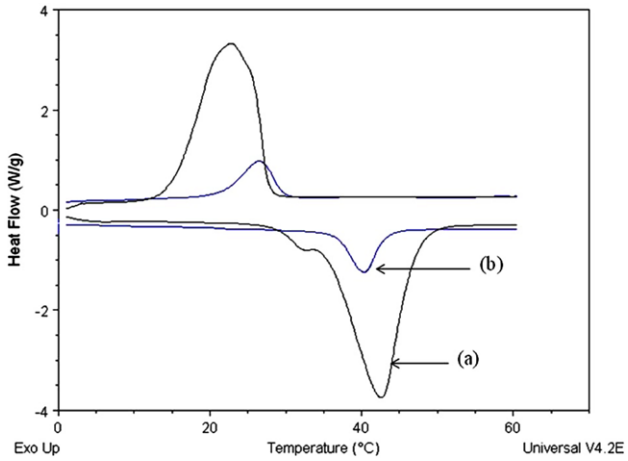

Figure 7. DSC curves of (a) PEG and (b) PEG/PVDF core/sheath non-woven mat fabricated at core and sheath feed rates of 0.108 and 1 mL/h, respectively.

of the core fluid and sheath fluid were 0.108 and 1 mL/h, respectively. The thermal properties of this non-woven mat, such as melting point, crystallization point, and latent heat, were measured by DSC. Figure 7 shows the DSC thermograms of pure PEG and the PEG/PVDF core/sheath non-woven mat fabricated at a core feed rate of 0.108 mL/h. The DSC thermograms indicate that the PEG/PVDF core/sheath non-woven mat melted at 36.2 ºC and crystallized at 29.7 ºC, while the melting and crystallization points of pure PEG were 34.9 and 27.6 ºC, respectively. The differences between the melting and crystallization points of the PEG/PVDF core/sheath non-woven mat and pure PEG were small (6.5 and 7.3 ºC, respectively). According to Mondal,[7] the difference between the melting and solidification points of a PCM should essentially be small so that the PCM can be used for obtaining a high efficiency thermal system, especially in the case of textile applications. The latent heats of melting and crystallization of the PEG/PVDF core/sheath non-woven mat were measured to be 34.8 and -31.3 J/g, respectively. The encapsulation ratio of PEG encapsulated in the core of the PEG/PVDF core/sheath non-woven mat was calculated by the ratio of the enthalpy values of the PEG/PVDF core/sheath non-woven mat and that of pure PEG as following equation:

$$\%\text{PEG} = \frac{\Delta H_{PEG/PVDF}}{\Delta H_{PEG}} \quad (1)$$

where $\Delta H_{PEG/PVDF}$ and ΔH_{PEG} are the measured latent heats of melting of the PEG/PVDF core/sheath non-woven mat and pure PEG, respectively.

From eq. (1), the encapsulation ratio of PEG of the core/sheath non-woven mat was calculated to be 20 wt%. Higher PCM ratios have been obtained by microencapsulation and melt coaxial electrospinning. PMMA/docosane microcapsules encapsulating 28 wt% docosane were fabricated by

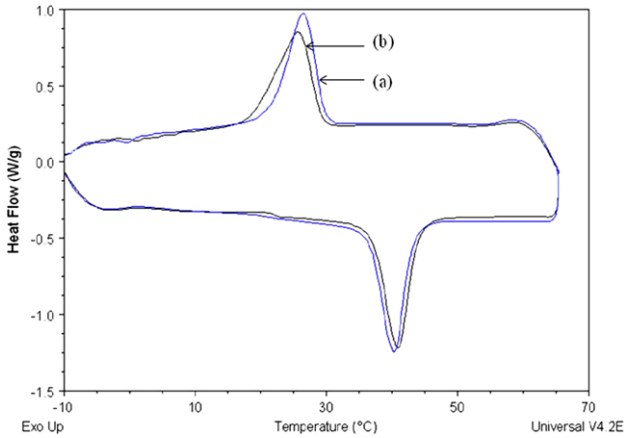

Figure 8. DSC curves of PEG/PVDF core/sheath non-woven mat fabricated at core and sheath feed rates of 0.108 and 1 mL/h, respectively, (a) before and (b) after 100 thermal cycles.

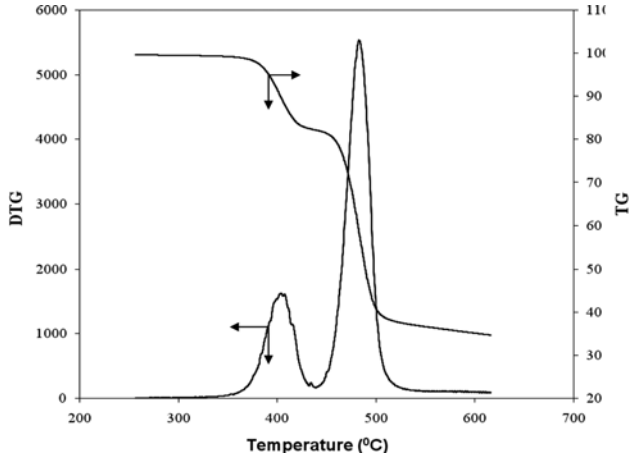

Figure 9. TGA thermogram of PEG/PVDF core/sheath non-woven mat fabricated at core and sheath feed rates of 0.108 and 1 mL/h, respectively.

Alkan *et al*..[14] By using the same method, Sarl *et al*.[5] achieved an encapsulation ratio of 43 wt% for octacosane and a PMMA shell. McCann *et al*. developed a method based on melt coaxial electrospinning for fabricating PCMs with up to 45 wt% octadecane.[21]

The thermal reliability of a PEG/PVDF core/sheath non-woven mat was also investigated by DSC analysis (100 thermal cycles), as shown in Figure 8. The corresponding thermal properties of pure PEG and a PEG/PVDF core/sheath non-woven mat before and after 100 thermal cycles are summarized in Table III. From these, it could be seen that after 100 thermal cycles, the melting point increased by 0.5 °C, while the crystallization point decreased by 0.5 °C. The latent heat of melting of the PEG/PVDF core/sheath non-woven mat decreased from 34.8 to 33.7 J/g, while the latent heat of crystallization decreased from 31.3 to 30.4 J/g. From these results, it could be confirmed that there was no significant changes in the melting and crystallization point or latent heat of the PEG/PVDF non-woven mats even after 100 heating-cooling cycles and that the PEG/PVDF core/sheath non-woven mat showed good thermal reliability.

Figure 9 shows a TGA thermogram obtained for the PEG/PVDF core/sheath nonwoven mat fabricated at core and sheath feed rates of 0.108 and 1 mL/h, respectively. A summary of the degradation temperatures and weight loss percentages of pure PEG, PVDF non-woven mat, and PEG/PVDF core/sheath non-woven mat are shown in Table IV. Figure 9 indicates that the PEG/PVDF core/sheath non-woven mat underwent degradation in two steps. On the basis of the data provided in Table IV, the first step was attributed to the degradation of PEG. Degradation of pure PEG started at around 280 °C while that of the PEG in the core of the PEG/PVDF core/sheath non-woven mat started at a higher temperature (300 °C). This implies that the degradation of PEG was slightly affected by PVDF present in the sheath encapsulating the core. After almost all the PEG in the nanofiber core degraded, PVDF in the sheath started to degrade (second step, at 431 °C). The degradation steps corresponding to PEG and PVDF could be easily distinguished from each other because of the large difference in the melting points of the two materials. The TG curve in Figure 9 shows that the weight loss percentage for the PEG encapsulated in the PEG/PVDF core/sheath non-woven mat was 21 wt%. This value was similar to the PEG ratio in the PEG/PVDF core/sheath non-woven mat (calculated from eq. (1) using the enthalpy values). This result indicates that in the core/sheath structure, the PVDF sheath had no remarkable effect on the latent heat of PEG in the core.

Mechanical Property. The main purpose of this study is the fabrication of nanofibers in which PEG (a PCM) is encapsulated by a PVDF sheath. PVDF plays the role of a protective polymer and helps maintain the shape of the fibers and prevent the leakage of PEG during phase change.

Table III. Thermal Properties of Pure PEG and PEG/PVDF Core/Sheath Non-Woven Mat Fabricated at Core and Sheath Feed Rates of 0.108 and 1 mL/h, Respectively, before and after 100 Thermal Cycles

Type of Sample	Cycle No.	Melting Point (°C) (Onset Temperature)	Latent Heat of Melting (J/g)	Crystallization Point (°C) (Onset Temperature)	Latent Heat of Crystallization (J/g)
PEG		34.9	171.9	27.6	168.0
PEG/PVDF Core/Sheath Non-Woven Mat	1 cycle	36.2	34.8	29.7	31.3
	100 cycles	36.7	33.7	29.2	30.4

Table IV. TGA Data for Pure PEG, Pure PVDF, and PEG/PVDF Core/Sheath Composite Non-Woven Mat Fabricated at Core and Sheath Feed Rates of 0.108 and 1 mL/h, Respectively, before and after 100 Thermal Cycles

Type of Sample	Degradation Temperature Range (°C)	Weight Loss (%)
PEG	280 to 440	100
PVDF	400 to 600	65
PEG/PVDF Core/Sheath Non-Woven Mat	300 to 431	21
	400 to 600	54

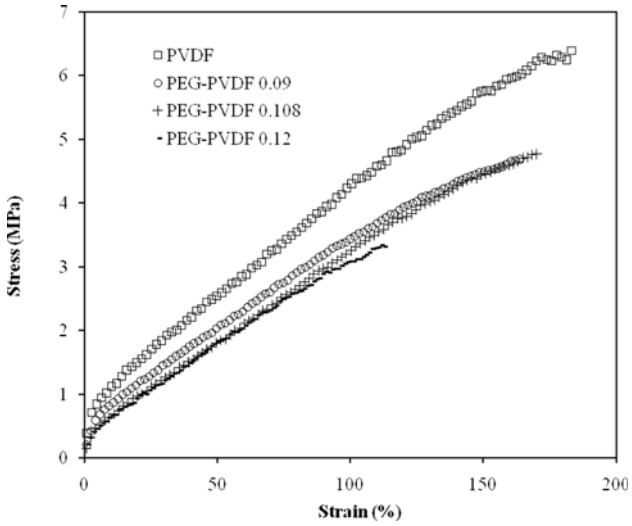

Figure 10. Mechanical properties of PVDF non-woven mat and PEG-PVDF non-woven mats fabricated by coaxial electrospinning at difference core feed rates.

Further, because of the presence of PVDF, the PEG/PVDF core/sheath non-woven mat is expected to show excellent mechanical performance. Figure 10 shows the tensile strength of the PVDF non-woven mat and PEG/PVDF non-woven mats fabricated by coaxial electrospinning at different core feed rates.

From this figure, it could be seen that the strain and stress of the PEG/PVDF core/sheath non-woven mats fabricated by the coaxial electrospinning were lower than those of the PVDF non-woven mat. The decrease in the tensile strength of the PEG/PVDF non-woven mats could be attributed to the inclusion of PEG, which has low tensile strength. However, the degree of elongation of the PEG/PVDF core/sheath non-woven mat electrospun at a core feed rate of 0.12 mL/h was much smaller than that of the PEG/PVDF core/sheath non-woven mats electrospun at core feed rates of 0.09 and 0.108 mL/h. This in turn was attributed to the poor core/sheath structure of the PEG/PVDF non-woven mat electrospun at core feed rate of 0.12 mL/h. From the results of WCA measurements and ATR FTIR, it was confirmed that PEG/PVDF core/sheath nanofibers cannot be obtained at a core feed rate of 0.12 mL/h. The presence of PEG in the PVDF sheath layer of the PEG/PVDF mat brought about a marked decrease in the degree of elongation.

Conclusions

Core/sheath non-woven mats comprising PEG 1000 (PCM) as the core and PVDF as the sheath layer were prepared by coaxial electrospinning. WCA measurements, ATR-FTIR analysis, XPS analysis, and TEM observations confirmed that PEG/PVDF core/sheath non-woven mats could be fabricated by appropriate adjustment of the core feed rates (0.09 and 0.108 mL/h) for a sheath feed rate of 1 mL/h. As shown in the FE-SEM images, PEG/PVDF core/sheath nanofibers with a broad diameter distribution and an average fiber diameter of approximately 700 nm were obtained by coaxial electrospinning. DSC analysis involving 100 melting/crystallization thermal cycles was carried out on the PEG/PVDF core/sheath nanofibers; the results revealed that the fibers underwent negligible change after heating, thus confirming the high thermal reliability of the PEG/PVDF core/sheath non-woven mats. The TGA thermogram of the prepared non-woven mats showed two separate degradation peaks for PEG and PVDF. Both DSC and TGA analyses showed that the PEG/PVDF core/sheath non-woven mats consisted of 20 wt% PEG. The PEG/PVDF core/sheath non-woven mats delivered a remarkable mechanical performance, implying that they have potential applications in the manufacture of smart textiles and solar energy storage materials.

Acknowledgements. This research was supported by Basic Science Research Program through the National Research Foundation of Korea (No. 20100011528). We thank Ms. Hye-Jin Cho of the Division of Electron Microscopic Research, Korea Basic Science Institute for her assistance in recording TEM images.

References

(1) C. Voelker, O. Kornadt, and M. Ostry, *Energ. Buildings*, **40**, 937 (2008).
(2) M. F. Dermirbas, *Energ. Source Part B*, **1**, 85 (2006).
(3) A. M. Khudhair and M. M. Farid, *Energ. Convers. Manage.*, **45**, 263 (2004).
(4) M. M. Kenisarin, *Renew. Sust. Energ. Rev.*, **14**, 955 (2010).
(5) A. SarI, C. Alkan, A. Karaipekli, and O. Uzun, *Sol. Energy*, **83**, 1757 (2009).
(6) N. Sarier and E. Onder, *Thermochim. Acta*, **452**, 149 (2007).
(7) S. Mondal, *Appl. Therm. Eng.*, **28**, 1536 (2008).
(8) C. Chen, L. Wang, and Y. Huang, *Polymer*, **48**, 5202 (2007).
(9) H. Zhang and X. Wang, *Colloids Surf. A*, **332**, 129 (2009).
(10) M. Jiang, X. Song, G. Ye, and J. Xu, *Compos. Sci. Technol.*, **68**, 2231 (2008).

(11) L. Bayés-García, L. Ventolà, R. Cordobilla, R. Benages, T. Calvet, and M. A. Cuevas-Diarte, *Sol. Energ. Mat. Sol. C*, **94**, 1235 (2010).
(12) R. Yang, Y. Zhang, X. Wang, Y. Zhang, and Q. Zhang, *Sol. Energ. Mat. Sol. C*, **93**, 1817 (2009).
(13) A. Pasupathy, R. Velraj, and R. V. Seeniraj, *Renew. Sust. Energ. Rev.*, **12**, 39 (2008).
(14) C. Alkan, A. SarI, A. Karaipekli, and O. Uzun, *Sol. Energ. Mat. Sol. C*, **93**, 143 (2009).
(15) C. Chen, L. Wang, and Y. Huang, *Mater. Lett.*, **63**, 569 (2009).
(16) C. Chen, L. Wang, and Y. Huang, *Mater. Lett.*, **62**, 3515 (2008).
(17) N. Bhardwaj and S. C. Kundu, *Biotechnol. Adv.*, **28**, 325 (2010).
(18) Z. M. Huang, Y. Zhang, and S. Ramakrishna, *J. Polym. Sci. Part B: Polym. Phys.*, **43**, 2852 (2005).
(19) A. Frenot and I. S. Chronakis, *Curr. Opin. Colloid. In.*, **8**, 64 (2003).
(20) G. C. Rutledge and S. V. Fridrikh, *Adv. Drug. Deliver. Rev.*, **59**, 1384 (2007).
(21) J. T. McCann, M. Marquez, and Y. Xia, *Nano Lett.*, **6**, 2868 (2006).
(22) A. Sharma, V. V. Tyagi, C. R. Chen, and D. Buddhi, *Renew. Sust. Energ. Rev.*, **13**, 318 (2009).
(23) V. V. Tyagi and D. Buddhi, *Renew. Sust. Energ. Rev.*, **11**, 1146 (2007).
(24) R. Baetens, B. P. Jelle, and A. Gustavsen, *Energ. Buildings*, **42**, 1361 (2010).
(25) Y. Jiang, E. Ding, and G. Li, *Polymer*, **43**, 117 (2002).
(26) Q. Meng and J. Hu, *Sol. Energ. Mat. Sol. C*, **92**, 1260 (2008).
(27) W. Ji, F. Yang, J. J. J. P. van den Beucken, Z. Bian, M. Fan, Z. Chen, and J. A. Jansen, *Acta. Biomater.*, in press, Uncorrected Proof.
(28) D. Liang, B. S. Hsiao, and B. Chu, *Adv. Drug. Deliver. Rev.*, **59**, 1392 (2007).
(29) Z. Sun, E. Zussman, A. L. Yarin, J. H. Wendorff, and A. Greiner, *Adv. Mater.*, **15**, 1929 (2003).
(30) Y. Xin, Z. Huang, W. Li, Z. Jiang, Y. Tong, and C. Wang, *Eur. Polym. J.*, **44**, 1040 (2008).
(31) K. H. K. Chan and M. Kotaki, *J. Appl. Polym. Sci.*, **111**, 408 (2009).
(32) B. Sun, B. Duan, and X. Yuan, *J. Appl. Polym. Sci.*, **102**, 39 (2006).
(33) X.-J. Han, Z.-M. Huang, C.-L. He, L. Liu, and Q.-S. Wu, *Polym. Composite*, **29**, 579 (2008).
(34) P. Zhao, H. Jiang, H. Pan, K. Zhu, and W. Chen, *J. Biomed. Mater. Res. A*, **83A**, 372 (2007).
(35) H. Jiang, Y. Hu, P. Zhao, Y. Li, and K. Zhu, *J. Biomed. Mater. Res. B*, **79B**, 50 (2006).
(36) C.-L. He, Z.-M. Huang, and X.-J. Han, *J. Biomed. Mater. Res. A*, **89A**, 80 (2009).